ACCELERATOR PROGRESS REPORT

FEATURE ARTICLE

SRILAC is Go!

Photo : Superconducting acceleration cavity for SRILAC

First Beam from SRILAC

RILAC upgrade project—Background and overview

The synthesis and naming of the 113th element, nihonium, is one of RIKEN's most noteworthy achievements; further, it has had a social impact in that the new element from Japan was added to the periodic table of elements.[1–3] This element was produced by the RIKEN heavy-ion linac (RILAC),[4] which has been in operation since 1980 as an injector to the RIKEN ring cyclotron (RRC) and for stand-alone applications such as those in atomic physics. In 1996, RILAC was upgraded to increase the beam intensity in RRC,[5–7] and in 2001, a booster linac[8] was installed as part of the RI Beam Factory (RIBF) project[9] under financial support from CNS, the University of Tokyo. This final step allowed nuclear physics experiments to be conducted in the RILAC facility.

Following the success of nihonium, research collaborations led by RIKEN scientists have set the next project of synthesizing new elements of atomic numbers greater than 118. To this end, metal ion beams such as vanadium and chromium need to be accelerated. However, the production cross section is expected to drop to less than a quarter of that for producing nihonium, and therefore, beam intensities need to be increased. In addition, it was estimated that the acceleration energy will need to be increased. Therefore, we need to increase the acceleration voltage of RILAC and beam intensity to initiate the project of synthesizing the new element.

Large accelerator facilities have contributed to society in the recent year in addition to promoting basic science such as research on super heavy element (SHE). At RIBF, several efforts have been invested in producing and distributing radioisotopes for research. One of the most popular isotopes is ^{211}At, and its production using AVF cyclotrons is being actively pursued for future medical applications.[10] ^{211}At has a short half-life of approximately 7 h, and a high-intensity beam of particles is essential for mass production. However, the technology for the mass production of ^{211}At has not been established. Therefore, the establishment of a technology for the mass production of useful isotopes has been added to the objectives of the RILAC upgrade plan.

The RILAC upgrade project (Fig. 1), which aims to synthesize new elements and develop technology for the mass production of useful radioisotopes, was approved with a supplementary budget in FY2016. Indeed, this enhancement plan will lead to a considerably higher intensity of the beam to the RRC, especially the metal ion beam, compared to that before.

The target performance expected in this upgrade program is to accelerate ions with $M/q = 6$ to $E = 6.5$ MeV/nucleon at more than 2.5 particle μA. To achieve this goal, we first built a new ion source. The structure of the ion source is almost identical to the

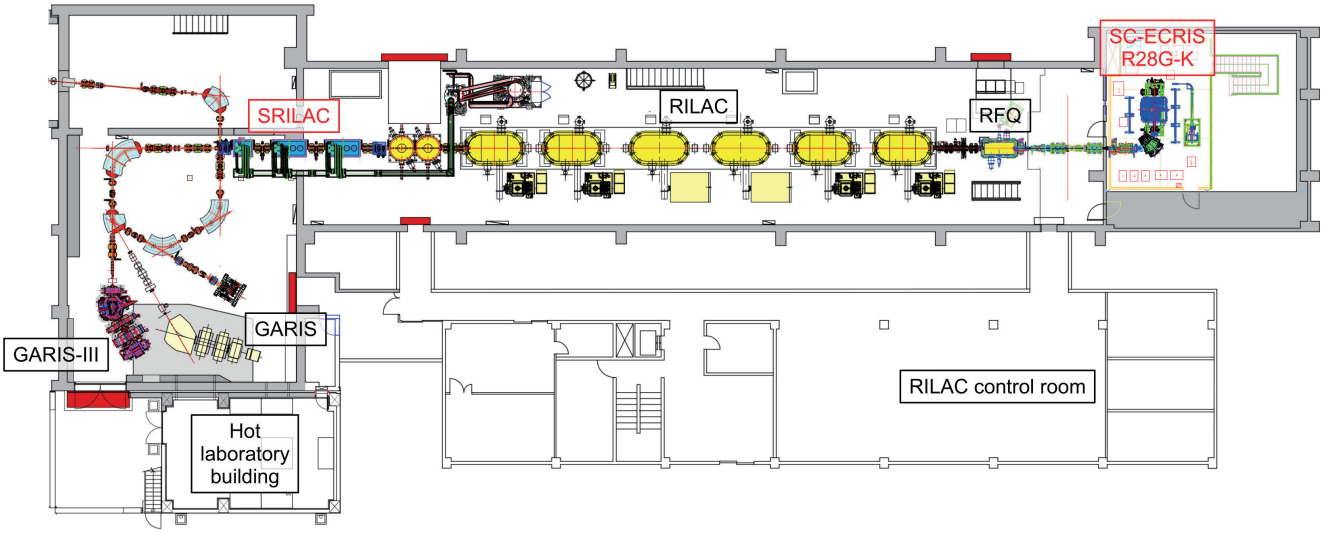

Fig. 1. Overview of RILAC upgrade project. 18-GHz ECRIS was replaced by R28G-K, and a downstream part of RILAC was replaced by SRILAC.

28-GHz superconducting electron cyclotron resonance ion source (SC-ECRIS) that has been operational since 2010.[11] There is a risk of damage to SC cavities in the downstream caused by the high-intensity beams. Therefore, we decided to limit the emittance in the low energy beam transport (LEBT) section up to the radio frequency quadrupole (RFQ) by measuring the beam emittance effectively.

Second, we replaced the last four normal conducting cavities in the RILAC booster with ten SC cavities to increase acceleration energy. Quarter-wavelength resonators (QWRs) were used as the SC cavities. A frequency of 73.0 MHz, which is four times the fundamental frequency of the RIBF, was selected for the SC cavities. This frequency is selected considering its future application as an RIBF injector. For the SC-QWR, we developed a 75.5 MHz QWR that cooperates with KEK under the ImPACT program since FY2014.[12] This experience has been of great help in the upgrade project.

In addition to the ion source, SC cavities, and refrigerator, test facilities of the cavities and a new hot laboratory building for processing radioisotopes were constructed. Further, a gas-filled recoil ion separator (GARIS) -II was moved from the RILAC facility to the E6 room in the Nishina Memorial Building to start the SHE experiments as soon as possible.[13] Meanwhile, the RRC resonator was modified to solve the problem of insufficient voltage at the RRC,[14] which had been a bottleneck in increasing beam intensity. This modification greatly contributed to the large increase in the uranium beam intensity for the BigRIPS experiments.

The construction of the ion source completed in March 2018 and the installation of the SC cavity in March 2019; this was followed by the construction of the control system of the SC cavities and the commissioning of the refrigerator in September 2019. The first beam was delivered on January 28, 2020 and the facility inspection was conducted on March 30, 2020, which marked the completion of the construction plan on schedule and within budget. This project could not have been accomplished without the help of the related manufacturers, KEK for the collaborative research, administrative staff for the many orders, and the management of the Nishina Center. We thank everyone who supported this project.

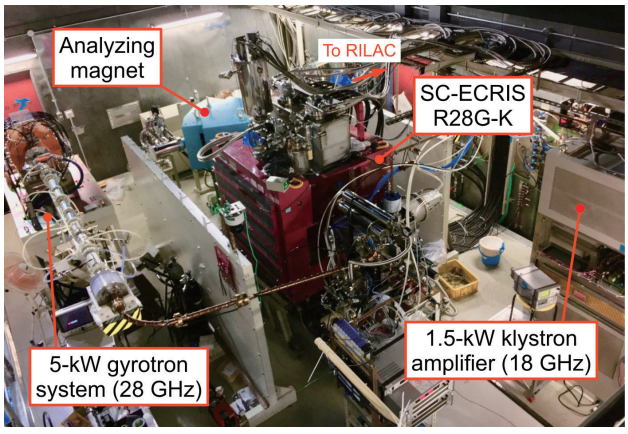

Fig. 2. Photograph of R28G-K and microwave generators (18-GHz klystron amplifier and 28-GHz gyrotron system). Extracted ion beams are analyzed by the dipole magnet and transported to the accelerator cavities of RILAC.

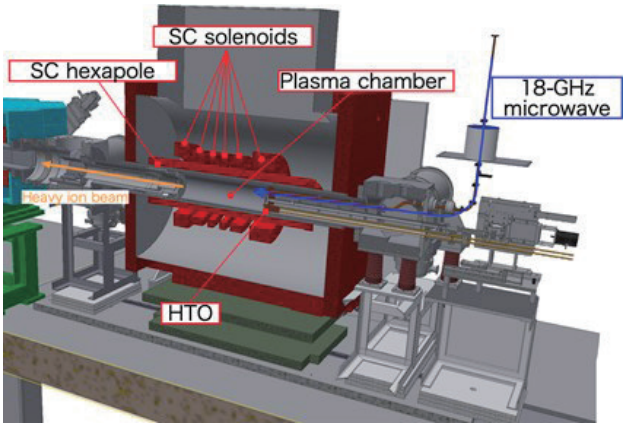

Fig. 3. Schematic cross section of the R28G-K. The large volume plasma chamber is surrounded by six SC solenoidal and one SC hexapole magnets. Both the 18- and 28-GHz microwaves are injected from the right side of the plasma chamber. The HTO is mounted on the injection side of the plasma chamber.

28-GHz Superconducting ECR Ion Source for RILAC

We constructed a 28-GHz SC-ECRIS as an essential part of the RILAC upgrade that began in FY2016. An ECRIS confines a hot electron plasma in which electrons are heated by microwaves through the ECR in a "magnetic field well." That is, a "magnetic mirror field" created by a combination of solenoidal and hexapole magnets known as the minimum-B configuration.[15] Multiple charged heavy ions are created by countless collisions of ions with sufficiently high-energy electrons in plasma. In the next projects at RILAC such as the search for new SHE with atomic number $Z > 118$ and RI production, it is necessary to provide unprecedented high-intensity ion beams. This means that it is necessary to confine the electron plasma, which has a higher density and a higher temperature than the plasma generated in the ECRIS used in RILAC, in a stable manner. Therefore, as shown in Fig. 2, new SC-ECRIS named RIKEN 28-GHz SC-ECRIS "KURENAI" (R28G-K) equipped with fully SC magnets and a high-power microwave generator system was launched in 2018.

R28G-K is equipped with six SC solenoidal magnets and a SC hexapole magnet as shown in Fig. 3. The arrangement of the SC magnets was set by the Ion source team of RIKEN Nishina center[11,16] based on previous research.[17–19] The SC coils are fabricated from Nb-Ti alloy and immersed in liquid He (more than 300 L) maintained in a high-power cryostat system combined with two 10-K GM (RDK-408S, SHI ltd.) and one 4-K GM (RDK-408D2, SHI ltd.) cryocoolers. Further, a GM-JT cryocooler (4 W at 4 K, SHI ltd.) is used to remove the excess heat induced by the large amounts of highly energetic X-ray radiation from the plasma. The maximum magnetic field of microwave injection side (B_{inj}), beam extraction side (B_{ext}), and radial magnetic field at the plasma chamber surface (B_{r}) are 3.8, 2.4, and 2.1 T, respectively. Otherwise, the bottom of the "field well" B_{min} changes from 0.5 T to 1.0 T, which makes the microwaves with both frequencies of 18 GHz and 28 GHz available to induce ECR with suitable mirror ratios such as $B_{\mathrm{inj}}/B_{\mathrm{min}} \sim 4$, $B_{\mathrm{ext}}/B_{\mathrm{min}} \sim 2$–3, and $B_{\mathrm{r}}/B_{\mathrm{min}} \sim 2$–3. Further, the shape of the mirror field around the B_{min} area can be changed arbitrarily by using the six solenoidal magnets. In other words, the field gradient and size of the ECR region can be changed to study the effects on the ECR plasma to optimize the beam intensity with a higher charge state. Since the SC magnets can generate a strong and large mirror field, the plasma chamber is a large-capacity cylinder with an inner diameter of 150 mm and a length of 575 mm. A total of 10 L/min or more of cooling water flows through the chamber wall. The large volume of the plasma chamber increases not only the volume of plasma but also the confinement time of the ions in the plasma to achieve a higher charge state.

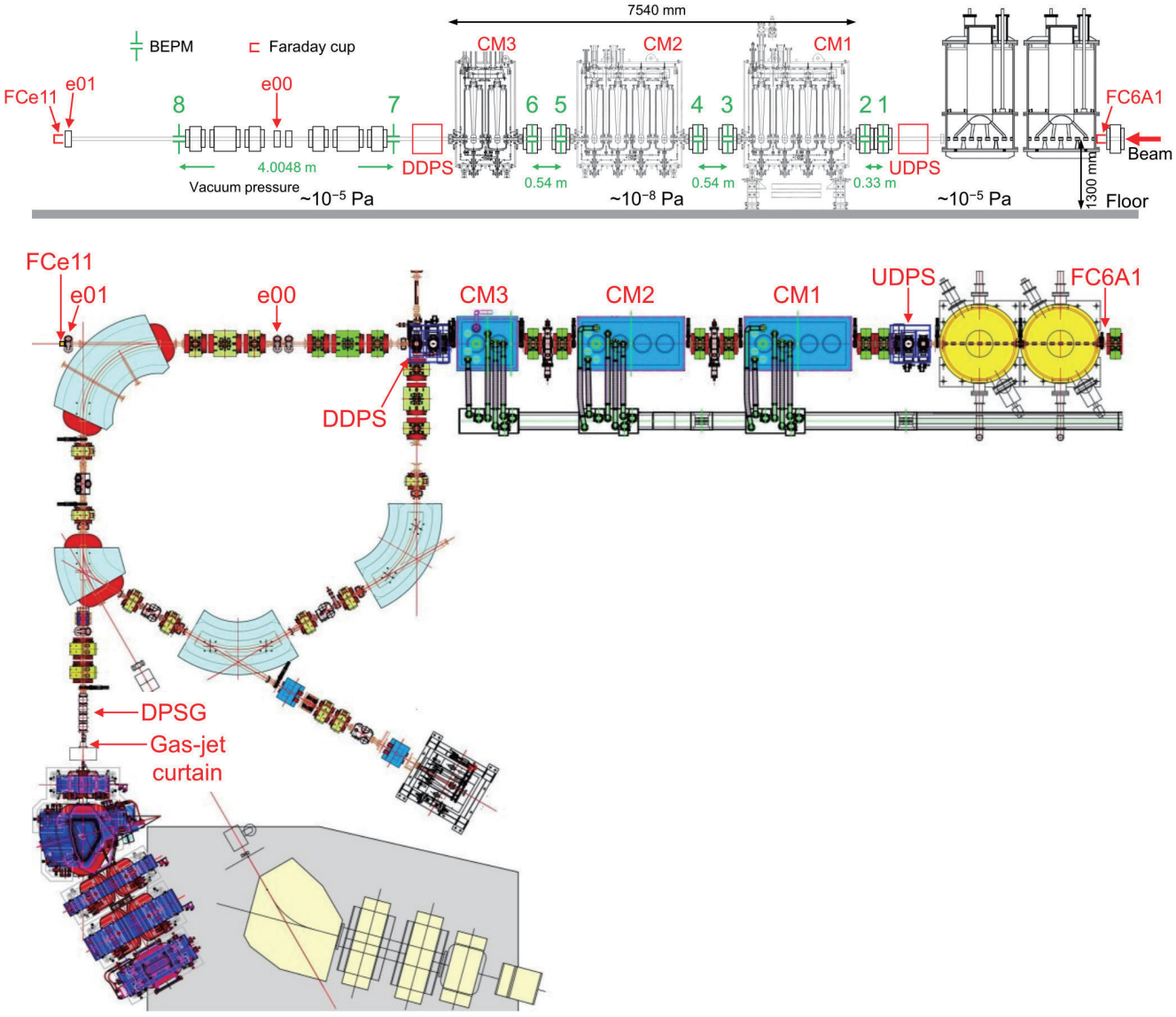

Fig. 4. Side and top views of the layout of SRILAC. Apparatuses described in the text are labeled.

The high-power microwave system contains a 1.5-kW klystron amplifier and 5-kW gyrotron for microwaves with frequencies of 18 GHz and 28 GHz, respectively. The high-power microwaves heat the electron in the plasma to remove the electrons bound deep inside the atoms or ions.

Recently, we have been developing a method to evaporate a solid material with a high melting point such as vanadium or calcium oxide using the high temperature oven (HTO).[20] The tungsten crucible of the HTO is heated to 2,000 K by the Joule heat caused by the high DC current of 700 A. For supplying the vanadium beam to search for the new SHE, the experiment lasted for about a month; therefore, we modified R28G-K so that two ovens could be used as described in the progress report this year.

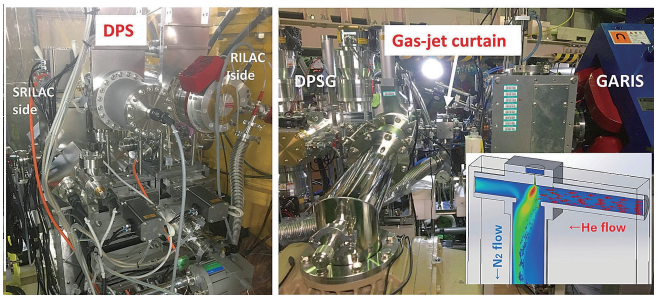

Fig. 5. Photographs of DPS (Left) and gas-jet curtain (Right).

Overview of SRILAC

The superconducting-RILAC (SRILAC) comprises three cryomodules (CM1, CM2, and CM3, see "SRILAC cryomodule" for detail), with room-temperature medium energy beam transport (MEBT) between them as shown in Fig. 4. The CMs contain neither SC magnets nor cold diagnostic devices. For the beam transport line connecting the CMs, the so-called MEBT, a newly designed beam energy position monitor (BEPM) is employed instead of traditional wire scanners and Faraday cups to avoid the generation of particulates that cause the degradation of the cavity performance (See "Beam energy position monitoring system for SRILAC" for detail). Further, to prevent the contamination of the SC parts where the vacuum pressure level is 1×10^{-8} Pa, it is important to have an isolation system between the existing room-temperature part where the vacuum pressure level is several 10^{-5} Pa and the SRILAC (See "Compact particle-removal differential-pumping system and N_2 gas-jet curtain for SRILAC" for detail).

Compact particle-removal differential-pumping system and N_2 gas-jet curtain for SRILAC

A compact non-evaporable getter-based differential pumping system (DPS) with electrostatic particle suppressors[21] has been developed to mitigate the large difference in the vacuum and clean conditions between the SRILAC and existing old RILAC with beamlines built almost four decades ago. The three-stage DPS was designed to achieve a pressure reduction from the existing beamline vacuum (10^{-6}–10^{-5} Pa) to an ultra-high vacuum of less than 10^{-8} Pa in SC cavities within a very limited length of only 75 cm, which ensures a beam aperture greater than 40 mm. All components (chambers, pumps, valves, vacuum gauges, etc.) were cleaned and assembled in an ISO class-1 clean room. The installation of the DPSs (UDPS and DDPS, See Figs. 4 and 5) was completed in December 2019. In operations during the past year, we confirmed that the DPSs achieved the desired pressure reductions in a stable manner without serious problems such as field emission problems.

During operations with GARIS-III for SHE research, He leakages to the SRILAC became an issue although a four-stage large DPS upstream of the GARIS (DPSG) was used for the windowless accumulation of He gas up to ∼70 Pa. The pressure of DDPS is increased to $\sim 10^{-7}$ Pa with the gas-filled GARIS-III when we use the narrow orifices of ϕ15 mm in the DPSG, which makes it difficult to transport high-intensity heavy-ion beams.

We introduced a N_2 gas-jet curtain downstream of DPSG (Figs. 4 and 5). The gas-jet curtain method is a new method introduced in the DPS of the He gas stripper.[22] This method suppresses the leakage of He gas by hitting a N_2-gas jet perpendicular to the He gas flow, and it converts the leaked gas into N_2 gas, which can be evacuated effectively with the DPS.

The gas-jet curtain system has a beam aperture with the diameter of ϕ25 mm. The nozzle is a two-dimensional Laval nozzle designed to generate an N_2-gas jet with a Mach number of 3.5 by optimizing with CFD calculations (Fig. 5).

In the tests with the GARIS team, we confirmed that there was no serious backflow of N_2 gas to the GARIS-III when the gas-jet curtain was under our operating conditions using a quadrupole mass analyzer. The effect of charge exchanges and energy losses of the injected beams by N_2 gas jet were confirmed to be negligible.

The installation of the gas-jet curtain was finished in September 2020. The leakage of He gas was significantly reduced with the N_2 gas-jet curtain and the pressure of the DDPS was $\sim 10^{-8}$ Pa even with larger orifices greater than ϕ25 mm in DPSG, which reduced the difficulties with high-intensity beam transport to the GARIS-III.

Table 1. Design parameters of SC-QWRs for SRILAC. The surface resistance is conservatively assumed to be 22.4 nΩ in the calculation.

Item	Value
Operating temperature	4.5 K
Frequency at 4.5 K	73.0 MHz
Duty	100%
E_{inj}	3.6 MeV/nucleon
E_{out}	6.5 MeV/nucleon
Maximum gap voltage	2.4 MV
Cavity type	QWR (TEM)
No. of SC cavities	10
Synchronous phase	$-25°$
β_{opt}	0.078
TTF	0.9
Aperture	ϕ40 mm
G	22.4 Ω
R_{sh}/Q_0	579 Ω
Target Q_0	1.0×10^9
Q_{ext}	$(1.0\text{–}4.5) \times 10^6$
P_0	8 W
E_{acc}	6.8 MV/m
V_{acc} at $E_{\mathrm{acc}} = 6.8$ MV/m, $\beta = 0.078$	2.16 MV
$E_{\mathrm{peak}}/E_{\mathrm{acc}}$	6.2
$B_{\mathrm{peak}}/E_{\mathrm{acc}}$	9.6 mT/(MV/m)
Amplifier output	7.5 kW
Beam current	∼100 electric μA

SRILAC cryomodule

The SRILAC comprises three CMs that contain a total of ten SC cavities.[23,24] CM1 and CM2 each contain four SC cavities, and CM3 contains two SC cavities (Fig. 4). The SC cavity of SRILAC is based on a coaxial QWR made of pure niobium. The resonant frequency is 73.0 MHz and the cavity is operated at 4.5 K cooled by liquid helium. The SC-QWR is fabricated using 3.5 mm and 4 mm pure niobium plates pressed together to make the top plate, stem, outer conductor, and bottom plate, and these are then assembled by electron beam welding. This is the first actual QWR made of pure niobium in Japan. Each QWR is designed to provide an acceleration voltage of 2.4 MV or higher at 8 W per unit. The design parameters of the cavity are summarized in Table 1.

Cross-sectional views of the QWR and CM are shown in Fig. 6. A pure titanium jacket is attached outside the cavity to store liquid helium. Permalloy is inserted into the space between the cavity and titanium jacket for magnetic shielding. The resonant frequency shifts because of external disturbances such as fluctuations in the liquid helium pressure. The tuner slightly pushes and deforms the cavity's beam port, which changes its capacitance and tunes its frequency to compensate for the slow shift. However, the frequency adjustment range of this tuner is 14 kHz towards lowering the resonant frequency, and therefore, the frequency variation is reduced by fine tuning the stem of each cavity and the total length of the outer conductor during assembly.[25]

The inner surface of the cavity was chemically polished to 110 μm after assembly, annealed at 750°C, and then chemically polished to 20 μm to maximize the performance of the SC cavity. The cavity was then high-pressure washed with ultrapure water from each port and vacuum sealed in an ISO class-1 clean room. After vacuum sealing, it was baked at 120°C, and performance tests were conducted on the single unit. As shown in Ref. 24), all ten actual cavities fabricated exceeded the target Q_0 value of 1×10^9 in the test. The cavity must be operated in compliance with the High

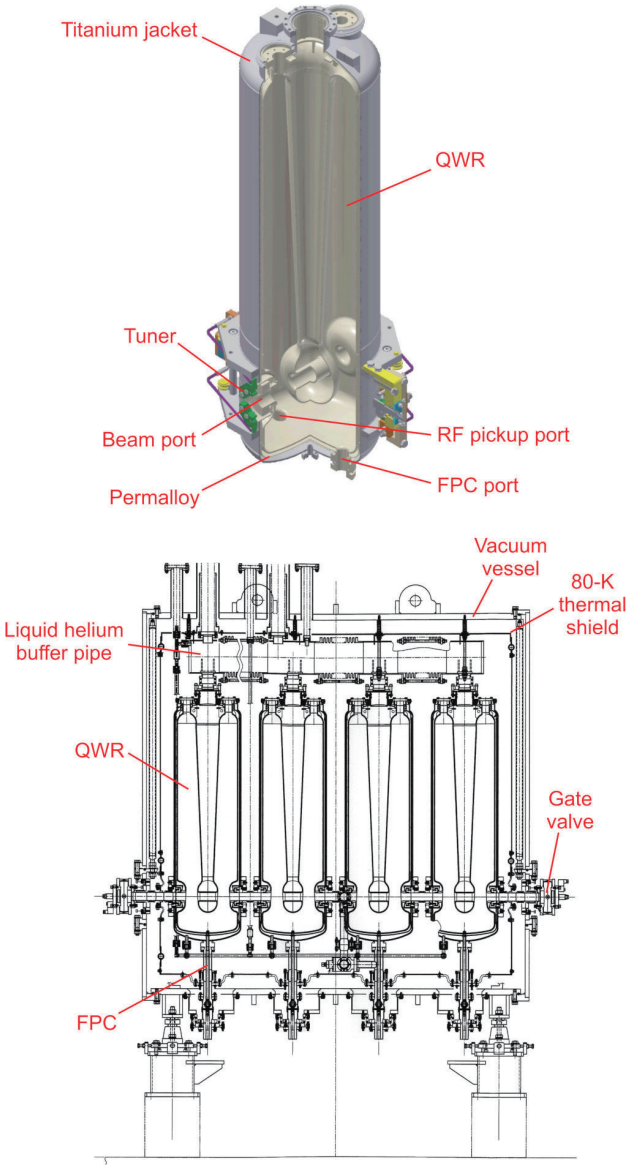

Fig. 6. Cross-sectional views of SC-QWR (top) and cryomodule that contains four SC-QWRs (bottom).

Pressure Gas Safety Act in Japan, and therefore, it was fabricated after preliminary evaluation and then commissioned for inspection.

A fundamental power coupler (FPC) and RF pickup are mounted on the bottom plate of the cavity. The FPC is a coaxial capacitively coupled type, vacuum sealed with a single ceramic window in the normal temperature section; it can handle the RF input power of 5 kW or more.[26] The FPC inner conductor is fabricated from oxygen-free copper, and the outer conductor from stainless steel with a copper plating on the inner surface. The thickness of the copper plating was determined by balancing heat penetration with the heat transfer to the low temperature side and heat generation caused by RF power.

The vacuum vessel of the CM is made of steel and divided into the top plate, top box, middle box, bottom box, and bottom plate. Electroless nickel plating was applied to prevent corrosion. The cavity is built with four glass-epoxy pillars on the bottom plate. One support is fixed in place, while the other three slide horizontally to allow for repositioning during cooling. Liquid helium buffer pipe is installed at the top of the cavity to control the liquid level for stable cooling. An aluminum plate is used for the 80-K thermal shield, which is cooled by liquid nitrogen flowing in series through three CMs. Cernox sensors are used as thermo sensors for the cavity, Pt-Co for the 4.5 K region, and Pt100 for the 80 K region. The heat load of the CM is estimated to be about 18 W for heat intrusion and about 32 W for RF loss in the cavity during steady state operation in a module containing four cavities. However, a heat load of 100 W per CM was set as the design standard value for operation during performance degradation.

The first step in assembling the CM is to move the bottom plate with the cavity and the middle box into the clean room and to fasten the cavity and beam pipe to seal their vacuum so that no dust can enter the cavity. Then, helium piping, liquid nitrogen piping, tuners, thermal shields, super insulators, etc. were installed, and the upper and lower boxes were covered after moving to the installation site (Fig. 7).

Fig. 7. Photographs of cryomodule. (Left) After assembling and sealing the cavities and beam pipes in the clean room. (Right) After alignment at the installation site.

Table 2. Requirements from cryomodules for SRILAC.

Item	Value
No. of SC cavities	10
No. of cryomodules	$2+1$
Temperature of SC cavities	4.5 K
Temperature of thermal shield	80 K
Weight of cold mass	1475 kg
Heat load to 4.5 K cold mass	
Dynamic	120 W
Static	30 W
Heat load to thermal shield	120 W
Cooling power	$\geq$500 W
Inventory	313 L
Design pressure of the He vessel	0.125 MPa(A)
Allowable pressure fluctuation	4.0×10^{-4} MPa

A total of ten sets of digital low-level RF (LLRF) circuits and 7.5 kW transistor amplifiers were introduced to excite the cavities. A digital low-level circuit is equipped with an FPGA that stabilizes the RF voltage and phase by PID control and obtains the tuning phase from the directional coupler signal. Internal parameters of the digital low-level circuit can be set remotely from a programmable logic controller (PLC). Transistor amplifiers can operate with full output reflection, and they are equipped with five 1.5 kW output units with built-in isolators to continue operation in the event of unit failure. A control system using the PLC is provided for each CM to control these RF equipment.

Cryogenic system for SRILAC

The requirements from CMs for the SRILAC are summarized in Table 2. SC cavities work at 4.5 K. The thermal shield is designed to be cooled down by liquid nitrogen, and the total weight of the cold mass is 1.5 ton. Heat load to 4.5 K and 80 K are 150 and 120 W, respectively. The inventory of liquid helium is 313 L and the allowable fluctuation of pressure in the SC cavities is as small as 4 hPa because a change in pressure can change the resonance frequency of the SC cavities. The design pressure of the vessel is as low as 0.125 MPa(A) because the cavity has bellow, which cannot sustain higher pressure.

The cryogenic system was designed to have a cooling power of 500 W at 4.5 K. This system comprises a helium compressor, refrigerator, and buffer tank. The cooling power is four times that of the heat load because we like to have a big margin to ensure contin-

uous operation even if the condition of the surface on the cavities is not so good that the cavities need considerably more cooling power. Figure 8 shows a cooling diagram of the cryogenic system. The compressed helium gas is introduced to a cold box and liquefied. Liquid helium is then supplied to the three headers in the CMs from the top. The evaporated cold helium gas is returned to the cold box and the helium compressor via heat exchangers. During pre-cooling, helium gas is supplied from the bottom to cool down the cavities efficiently. Green lines are used for liquid nitrogen supplied for shield cooling. A backup compressor for the superconducting ring cyclotron (SRC) was used for this cryogenic system to reduce the total cost. The required pressure fluctuation of 4 hPa looks tight; however, from experience, it is possible by control return pressure by the return valve with a precise pressure gauge. The Air Liquide company supplied devices for the cryogenic system other than the compressor. Radiation-resistant valve positioners were adopted because we install the refrigerator in the accelerator room.

The stand-alone operation of the helium refrigerator demonstrated a cooling capacity of 700 W at 4.5 K before the first cooling of the SRILAC. Figure 9 shows the cooling down curves. The cold mass was successfully cooled down to liquid helium temperature in four days although pre-cooling was halted because of the trouble in the thermal insulation vacuum system for half a day. The heat load was estimated from the heater in the helium refrigerator to be 150 W for $2+1$ CMs. The pressure fluctuation was hit within 4 hPa.

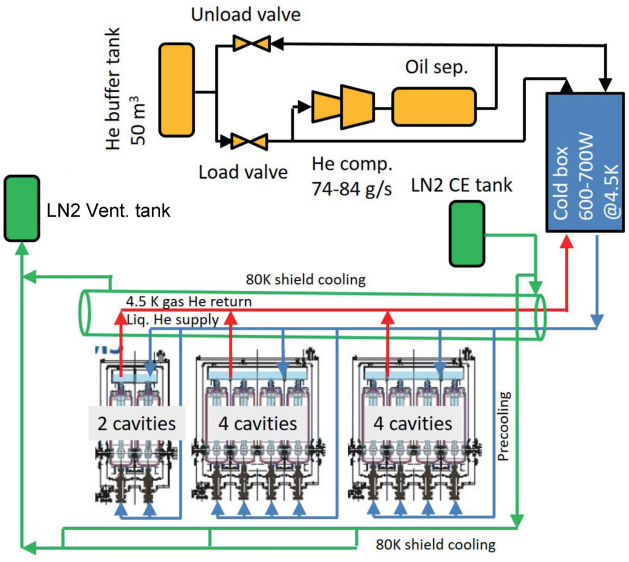

Fig. 8. Cooling diagram for SRILAC.

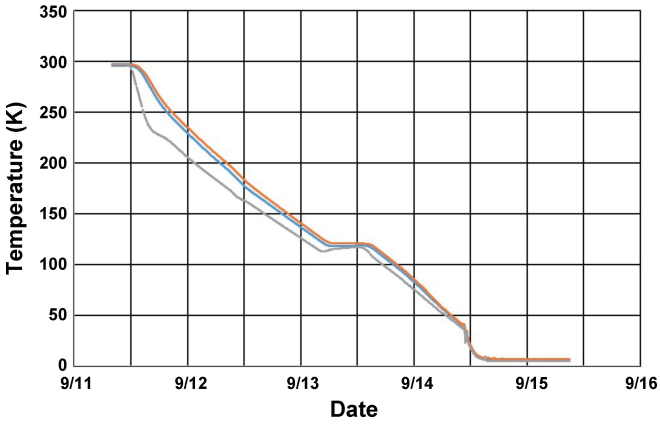

Fig. 9. Temperature of cold masses in the three CMs in the first cooling down.

Beam energy position monitoring system for SRILAC

It is crucial to monitor a beam to accelerate it stable manner. When the SRILAC beam is accelerated, beam loss must be reduced to under 1 W/m. Furthermore, destructive monitors generate outgassing; if they are used, it becomes difficult to maintain the Q-value and surface resistance of the SC cavities over a long period of time. Therefore, we developed a new BEPM system that can simultaneously measure the beam position and energy by measuring the time-of-flight (TOF) to continuously monitor the beam nondestructively. A great advantage of this system is that it can handle a time-chopped beam by synchronizing the measurement system with the beam-chopping signal. At the start of commissioning, the beam was chopped to several percent duty cycle to protect the SC cavity from beam loss. Although the beam intensity was 20 electric nA, we measured the beam position and energy to accuracies of ± 0.1 mm and several 10^{-4} precision, respectively.

Depending on the installation location, three types of BEPMs (Types I, II, and III) were designed and 11 BEPMs were fabricated. The BEPMs are installed in the centers of the quadrupole magnets located between the CMs. Photographs of three types of BEPMs and a cross section of a BEPM are shown in Fig. 10. The ideal linear response of the quadrupole moments is realized by using a parabolic design while maintaining good linear position sensitivity.

A block diagram of the BEPMs and data-acquisition (DAQ) system is shown in Fig. 11. The DAQ system can synchronize the RF reference with a beam chopper signal. The amplified pickup signals are transmitted through coaxial cables to the signal processing devices. The upstream and downstream signals are switched by multiplexers and digitized by digitizers (PXIe-5160). Although the sampling speed is 1.25 GS/s, a consider-

ably higher sampling speed of 50 GS/s can be achieved by using the random interleave mode under the condition that the signal is repeating continuously. Thus, highly accurate TOF measurements can be realized. All modules are integrated into a PXI express chassis. The signal process procedures are controlled by the LabVIEW 2019 graphical programming language, and module drivers are supported by the National Instruments Corporation. The obtained data are shared using the CA Lab that is a user-friendly, lightweight, and high-performance interface between the LabVIEW program language and EPICS-based control system. It allows easy reading and writing of EPICS process variables (PV). Measurement results are displayed on a remote desktop. Further, once these data are saved, the Control System Studio (CSS), which is an Eclipse-based tool to operate a large-scale control system, can display the results anywhere in the control room.

The first $^{40}Ar^{13+}$ beam acceleration commissioning was conducted using nine SC cavities. Figure 12 shows the displayed results of the BEPM measurements immediately after the beam was successfully accelerated to 6.2 MeV/nucleon (2020/01/28 21:02). The waveforms, beam positions, and beam energies at each station are displayed; the value circled in red indicates the final accelerated energy.

The BEPM system worked extremely well when determining phases of SC cavities and confirming beam energies and positions, which enabled stable beam acceleration. The measured beam energy is plotted in Fig. 13 as a function of the phase of the final SC cavity. In the focusing region, the lower energy beam gains

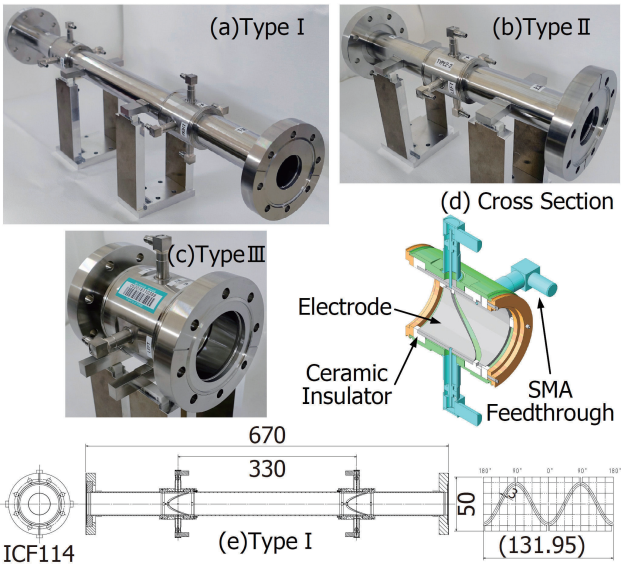

Fig. 10. Photographs of the three types of BEPMs: (a) Type I, (b) Type II, and (c) Type III. (d) Cross section drawing of a BEPM. (e) Schematic of Type I.[27]

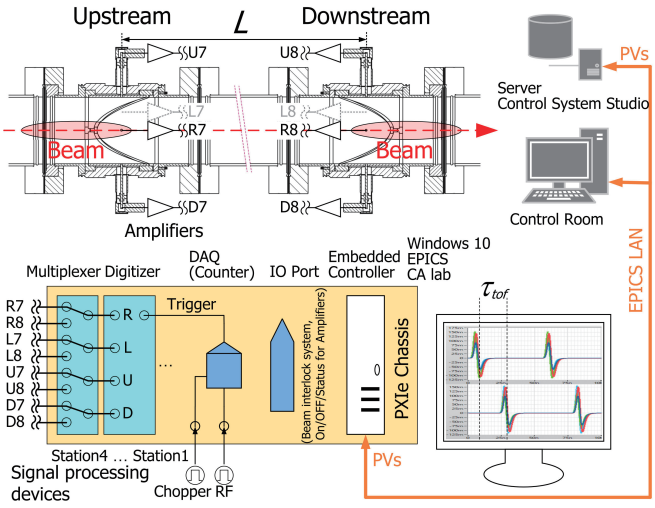

Fig. 11. Block diagram of BEPMs and DAQ system.[27]

energy, whereas in the defocusing region, the lower energy beam loses energy. This measurement clearly shows us the region we should select to accelerate the beam stably. The phases of SC cavities are currently set to −25°. Each phase of the SC cavity was measured and set in sequence from upstream to downstream (See "Beam Commissioning of SRILAC" for detail).

Overview of Control System for SRILAC Project

A distributed control system that uses Experimental Physics and Industrial Control System (EPICS) should be adopted as in RIBF to operate the SRILAC project efficiently, and a higher-level application protocol needs to be integrated to the EPICS Channel Access (CA) protocol. Further, the SRILAC control system requires corrections and upgrades to the shortcomings of previous RILAC control system, for example control protocol for an electromagnet power supply and a machine protection system.

In this project, the R28G-K was installed at the frontend of RILAC to increase the beam intensity. The new SC-ECRIS control system consists of PLCs embedded with EPICS.[28] The ion source control system differs from other control systems in that control stations with digital and analogue modules need to be installed on the high-voltage stage. At RIBF, a reliability of the conventional SC-ECRIS control system is not so high because interlock signals are exchanged via TCP/IP between the safety system and control stations on the high-voltage stage. The new SC-ECRIS control system uses two different types of CPUs (sequence CPU and Linux CPU) in the main PLC station, and it was connected to five PLC substations with a star-topology field bus communication using optical fibers for insulation. As a result, the interlock signal

exchanges the control station on the high-voltage stage through field bus communication on the optical fiber; system reliability was improved compared with the system that uses the TCP/IP-based interlock signal.

With this SRILAC project, the layout of the beamline has changed and new electromagnet power supplies have been introduced for the LEBT electromagnet. Old electromagnet power supplies were utilized for MEBT electromagnets. These electromagnet power supplies control used GPIB as the communication protocol, and their performance was relatively low compared with the modern protocol. Therefore, we upgraded the power supplies to replace the GPIB communication with the standard method of RIBF control system such as FA-M3 PLC and NIO.[29] In beam commissioning, approximately 30 modified electromagnet power supplies were controlled via EPICS CA protocol without problems.

With the installation of the SRILAC downstream of the normal conducting RILAC, a machine protection system has become necessary. For the previous RILAC control system, the machine protection system, which comprises a simple electromagnetic relay circuit has been implemented. The machine protection system is called the Beam Interlock System (BIS) at RIBF; further, we newly developed and implemented BIS for SRILAC. The BIS has a mechanism that activates the beam chopper for a signal triggered by an error from the control equipment and stops the beam. The speed at which the trigger signal is transmitted to the CPU is improved compared with that of the conventional BIS by adopting the field bus connection for inter-station communication. In addition, by adopting a ring-topology, we designed it to increase redundancy.

In the previous RILAC control system, hard-wired

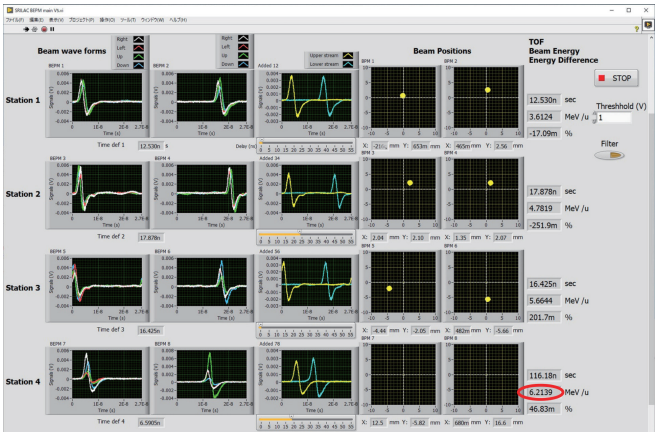

Fig. 12. Displayed BEPM measurement results immediately after the $^{40}Ar^{13+}$ beam was successfully accelerated to 6.2 MeV/nucleon (2020/01/28 21:02). Positions at station 4 were off scale, and it was corrected after the first trial acceleration.[27]

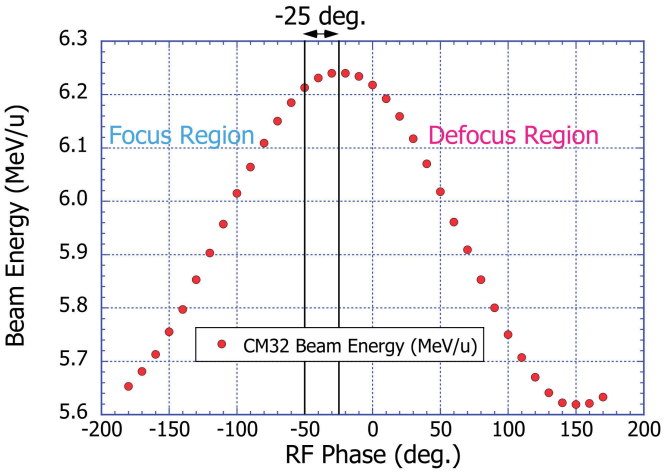

Fig. 13. Measured beam energy plotted as a function of the phase of the final SC cavity.[27]

control that directly connects the accelerator room and control room with a wire was already replaced and all operations were based on remote control. However, various systems such as data collection and RF control were not integrated with the EPICS CA protocol, and these were stand-alone systems. When the control system was updated in the SRILAC project, all control protocols for the higher-level application were integrated in the EPICS CA protocol. For example, BEPM was a LabVIEW-based system using National Instrument PXI, and by introducing CA Lab in the middle layer, we succeeded to operate it using the EPICS CA client.[27]

Since we succeeded to access to almost all control equipment including the above-mentioned electromagnet power supply, BIS, BEPM, and RF using the EPICS CA protocol, it had become possible to unify the development method of the operator interface (OPI) and realize various OPIs using CSS (Fig. 14). In addition, the Archiver Appliance has been newly introduced as the EPICS-based data archive system; it has become possible to store nearly 10,000 signal points as data at a cycle of 10 Hz or higher.[30] This system has the ability to search for arbitrary data by the timestamp and visualize the data on a Web-based application. During SRILAC beam commissioning, the Archiver Appliance was very useful for clarifying the behavior of SC cavity and the cause of troubles, and it is currently one of the essential tools for SRILAC beam tuning. In the RILAC control room (Fig. 1), consoles for hard-wired control system have been removed and new consoles ideal for the remote-control system have been introduced (Fig. 15).

In the near future, we plan to improve the performance of BIS and implement another type of machine protection system driven by the behavior of electri-

cal current for the electromagnet[31] because of the increase in the beam intensity from SRILAC.

Beam Commissioning of SRILAC

The design parameters of the SRILAC are listed in Table 1, and its layout is shown in Fig. 4. The TEM cavities for the SRILAC are designed to operate in the CW mode. The gap length of the cavity is optimized for $\beta = 0.078$ particles with a transit time factor of 0.9. The maximum gap voltage is 2.4 MV, which corresponds to an acceleration gradient E_{acc} of 6.8 MV/m with a synchronous phase of $-25°$.

The FPC is designed with a tunable coupling so that a Q_{ext} range from 1×10^6 to 4.5×10^6 can be achieved by changing the insertion distance of its antenna. The maximum beam current is about 100 electric μA for the SHE synthesis experiments; therefore, beam loading is negligible. A low Q_{ext} as small as 10^6 was selected to broaden the resonance curve with a ± 60 Hz operational-frequency-range achieved by an RF input power of 7.5 kW. In October 2019, the first RF test with an operational temperature of 4.5 K was performed without significant trouble, except SC05 encountered a vacuum leakage from the ceramic window of the coupler. During the RF test, amplitude feedback and phase-lock loop parameters of the newly developed digital LLRF were optimized and a stable RF-field was successfully obtained.

After a successful RF test, in January 2020, the beam acceleration test was conducted for the first time. An ^{40}Ar beam was accelerated based on the requirement for SHE synthesis experiments. However, one of the SC-QWRs (SC05) was not available; therefore, the acceleration energy was lowered to 6.2 MeV/nucleon from the designed energy of 6.5 MeV/nucleon.

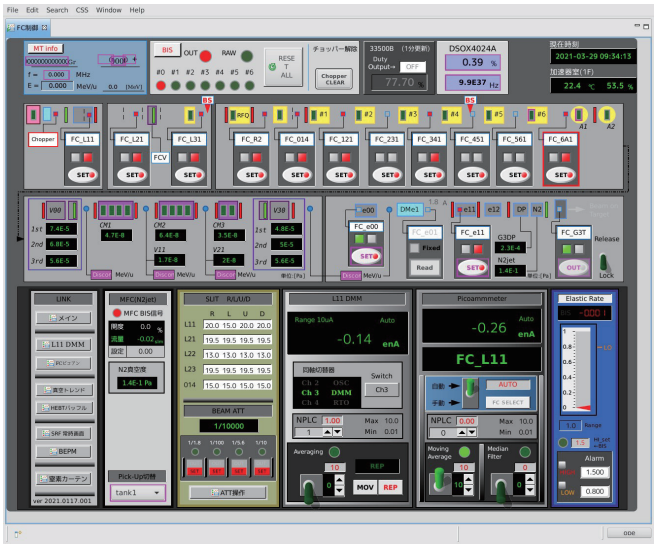

Fig. 14. Screenshot of CSS-based OPI for Faraday cup operation.

Fig. 15. New consoles for remote operation in the RILAC control room.

The $^{40}Ar^{13+}$ beam with an intensity of approximately 23 electric nA (duty 3%, chopper frequency 1 kHz) was accelerated to 6.2 MeV/nucleon with a gap voltage of 1.13 MV. For the SC-linac tuning, SC-QWRs were energized one-by-one and the beam energy was measured with a systematic variation of the RF-field phase (Fig. 16). The beam energy was precisely obtained by a TOF measurement with a pair of BEPMs with a low beam current as described above. The phase-scan plot, where E_{out} is plotted as a function of the RF-field phase for each cavity, is shown in Fig. 16. The synchronous phase $\phi_{\mathrm{s}} = -25°$ was obtained by shifting the RF-field phase from the zero acceleration/bunching phase by 65° towards the top of the sine curve. The beam position remained almost at the center of beam aperture during the phase scan because of the geometrical correction caused by the steering effect of the QWR cavity.[23] The accelerated beam energy successfully reached 6.2 MeV/nucleon at 9 PM on January 28, 2020.

After elaborate tuning, the transmission efficiency from FC6A1 to FCe11 in Fig. 4 reached 100% with a beam current of 6.11 electric μA. The vertical and horizontal beam positions monitored by BEPM were centralized and the beam loss which occurred at the MEBT was minimized keeping the deterioration of the vacuum pressure below 1×10^{-7} Pa.

A $^{51}V^{13+}$ beam with an energy from 4.2 MeV/nucleon to 6.3 MeV/nucleon was delivered for a user service time. To achieve a beam current of 10 particle μA, the transmission efficiency of the low-energy part of the RILAC and optimization of the beam transport of the SRILAC are currently being analyzed. The data archive system[30] for many accelerator parameters in-

cluding not only the RF-field of the RF cavities, but also the excitation current of the magnets, vacuum, temperature of the cooling water, and BEPMs, is very helpful to understand what occurs during beam tuning. Each cavity achieved the acceleration gradient of 5.7 MV/m that accelerates ions with M/q of 5.4 to 6.5 MeV/nucleon with ten cavities. The newly developed digital LLRF will be adopted to each RF system of the RT-DTLs, RFQ, and bunchers to improve the stability of their RF-field.

Beam transport optimization from SRILAC to GARIS-III

This section reports on beam transport. Heavy-ion beams accelerated to approximately 6 MeV/nucleon by SRILAC are transported to GARIS-III through the transport line called the high energy beam transport (HEBT) line. The configuration of the beam line is TQ–TQ–D–SQ–SQ–DQ (TQ = Triplet Quadrupole, D = Dipole, SQ = Singlet Quadrupole, DQ = Doublet Quadrupole) as shown in Fig. 4. Further, there is one dipole magnet between the second SQ and DQ, but this is not excited when the beam is transported to GARIS-III. The duct diameter is 60 mm in most places; however, it is narrowed to 15–25 mm just before the target because of DPSG.

The requirements for the beam transport of the HEBT line are (A) beam loss less than a few percent and (B) the adjustability of beam spot shape on the GARIS-III target depending on the experimental conditions. The first requirement is important for maintaining the outside radiation dose. Since the side wall of GARIS-III is relatively thin, it is necessary to measure and confirm the dose while optimizing beam transport. For the second requirement, a horizontal ellipse is desired in the production run to prevent the local depletion of the rotating target, while a large circle shape is desired in the calibration run. To satisfy these requirements, the beam envelope should be narrower just before the target, where there is a relatively smaller acceptance, and it should be wider at the target.

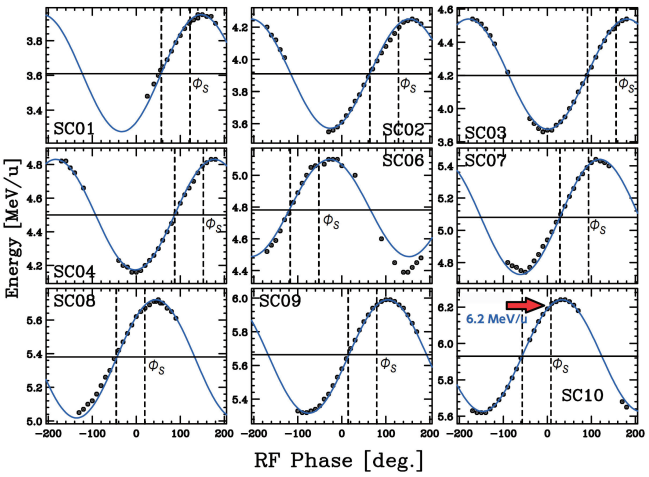

Fig. 16. Phase scan plot for first ^{40}Ar 6.2 MeV/nucleon acceleration test.

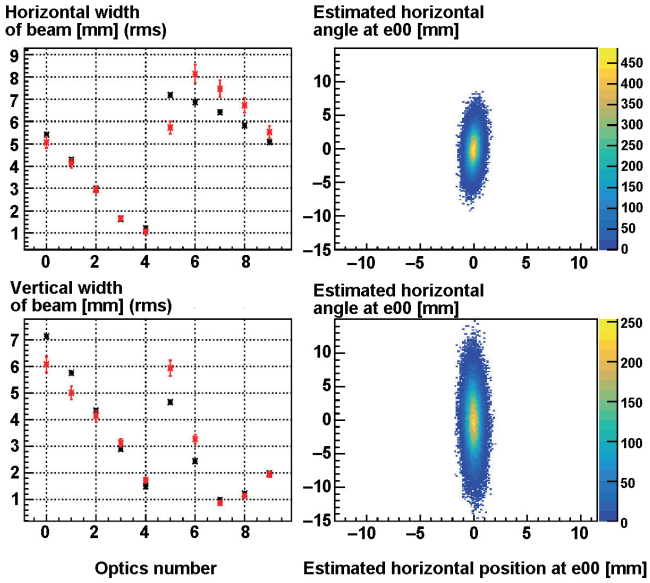

Fig. 17. Data of emittance measurement after phase-ellipse adjustment at an object point e00. (Left) Measured values (red dots) and fit results (black dots) of beam widths at the point denoted as e01. (Right) Phase ellipse estimated by fitting results. Top and bottom figures correspond to horizontal and vertical directions, respectively.

Detailed optical calculation is required according to the phase ellipse of the beam at that time to realize the ideal optics with a limited number of optical elements. The optics are adjusted in the following three steps. First, the phase ellipse of the beam at e00, which is defined as the object point in the optical design, is measured using the wire scanners at e00 and e01 (Fig. 4). The beam width at e01 is measured with several optics between e00 to e01 by changing the TQ magnets. Comparing the obtained widths and transfer matrices, the phase ellipse at e00 is estimated. Second, the phase ellipse at e00 is adjusted to be upright by the TQ upstream of e00 based on an optical calculation. Third, the optics from the object point to GARIS-III are tuned using optical simulation[32] based on an adjusted phase ellipse at e00 and an experimental requirement for beam spot shape. In the default optics, the position magnifications from e00 to GARIS-III are 1.0 in both of the horizontal and vertical directions. Based on the measured phase ellipse and experimental requirements, position magnifications are adjusted while suppressing the beam envelope in the entire beam line. Finally, the optical system is optimized with a few particle μA beam by fine-tuning the quadrupole magnets

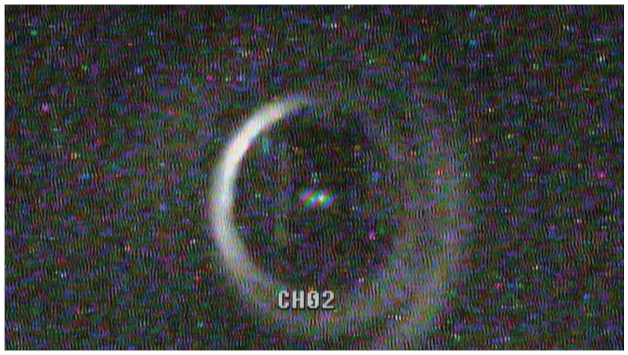

Fig. 18. Beam spot picture on viewer at GARIS-III target taken by CCD camera. The beam spot shape is a horizontal ellipse as expected.

and steerers based on the baffle inside the differential pumping system and viewer on the target.

Figure 17 shows an example of the estimated e00 phase ellipse after step 2, which causes the phase ellipse to be upright. This measurement was performed in a commissioning run in June 2020, in which Ar^{11+} accelerated to 5 MeV/nucleon with intensity of 30 electric nA was utilized. The graphs shown on the left represent the beam widths (rms) measured by the e01 wire scanner in each optics, the red dots represent the measurements, and black dots represent fit results. The contour plots shown on the right are phase ellipses at e00 estimated from the fit results. Here, the phase ellipses are assumed to be two-dimensional Gaussian distributions. As shown in the figures, the phase ellipses were adjusted to be upright as calculated. The horizontal 4 rms emittance was $\epsilon_{\rm h} = 3.1$ (πmm·mrad), and the vertical 4 rms emittance was $\epsilon_{\rm v} = 6.5$ (πmm·mrad), respectively. These values were consistent within 20% with the values before the phase-ellipse adjustment. The measurement and adjustment of the phase ellipses are almost automated except for the data acquisition by the wire scanners; they are completed in about an hour.

After the phase-ellipse adjustment, the optics from e00 to the GARIS-III target were optimized. As shown in Fig. 18, the beam spot on the target was tuned to be a horizontal ellipse, as expected for the rotation target. It was confirmed using Faraday cups that the beam loss was controlled within a few percent. Also leakage radiation was within the allowable range. In these adjustments, the calculation of optics and the application of calculated currents to magnets were automated; the optics optimization was completed in a few hours including the fine adjustment of the steerers.

Optics in the HEBT line was optimized as expected based on the phase ellipse measurement and optical simulation. A new method to estimate the phase ellipse with non-destructive detector BPEMs[33] is under development.

References

1) K. Morita *et al.*, J. Phys. Soc. Jpn. **81**, 103201 (2012).
2) P. J. Karol *et al.*, Pure Appl. Chem. **88**, 139 (2016).
3) `http://iupac.org/iupac-is-naming-the-four-new-elements-nihonium-moscovium-tennessine-and-oganesson/`.
4) M. Odera *et al.*, Nucl. Instrum. Methods Phys. Res. A **227**, 187 (1984).
5) A. Goto *et al.*, RIKEN Accel. Prog. Rep. **28**, 163 (1995).
6) T. Nakagawa *et al.*, Rev. Sci. Instrum. **71**, 637 (2000).
7) O. Kamigaito *et al.*, Rev. Sci. Instrum. **70**, 4523 (1999).
8) O. Kamigaito *et al.*, Rev. Sci. Instrum. **76**, 013306 (2005).
9) Y. Yano, Nucl. Instrum. Methods Phys. Res. B **261**, 1009 (2007).
10) Y. Wang *et al.*, RIKEN Accel. Prog. Rep. **53**, 192 (2020).
11) T. Nakagawa *et al.*, Rev. Sci. Instrum. **81**, 02A320 (2010).
12) N. Sakamoto *et al.*, Proc. 18th International Conference on RF Superconductivity (SRF2017), 681 (2017).
13) Y. Watanabe *et al.*, RIKEN Accel. Prog. Rep. **51**, 132 (2018).
14) K. Yamada *et al.*, RIKEN Accel. Prog. Rep. **52**, 13 (2019).
15) R. Geller, in *Electron Cyclotron Resonance Ion Sources and ECR Plasmas*, (IOP Publishing, Bristol, 1996) p. 121.
16) Y. Higurashi *et al.*, Rev. Sci. Instrum. **85**, 02A953 (2014).
17) G. D. Alton *et al.*, Rev. Sci. Instrum. **65**, 775 (1994).
18) M. A. Leitner *et al.*, Phys. Scr. **T92**, 171 (2001).
19) D. Hitz *et al.*, Rev. Sci. Instrum. **73**, 509 (2002).
20) J. Ohnishi, Proc. 23rd International Workshop on ECR Ion Source (ECRIS2018), 180 (2018).
21) H. Imao *et al.*, RIKEN Accel. Prog. Rep. **53**, 10 (2020).
22) H. Imao *et al.*, RIKEN Accel. Prog. Rep. **52**, 14 (2019).
23) N. Sakamoto *et al.*, Proc. 29th Linear Accelerator Conference (LINAC18), 620 (2018).
24) K. Yamada *et al.*, Proc. 19th International Conference on RF Superconductivity (SRF2019), 502 (2019).
25) K. Suda *et al.*, Proc. 19th International Conference on RF Superconductivity (SRF2019), 182 (2019).
26) K. Ozeki *et al.*, RIKEN Accel. Prog. Rep. **52**, 106 (2019).
27) T. Watanabe *et al.*, Proc. 9th International Beam Instrumentation Conference (IBIC2020), 295 (2020).
28) A. Uchiyama *et al.*, Rev. Sci. Instrum. **91**, 025101 (2020).
29) A. Uchiyama *et al.*, Proc. 16th Annu. Meet. Part. Accel. Soc. Jpn. (PASJ), 869 (2019).
30) A. Uchiyama *et al.*, Proc. 17th Annu. Meet. Part. Accel. Soc. Jpn. (PASJ), 739 (2020).
31) K. Kumagai *et al.*, RIKEN Accel. Prog. Rep. **52**, 115 (2019).
32) `https://web-docs.gsi.de/~weick/gicosy/`.
33) T. Watanabe *et al.*, Proc. 8th International Beam Instrumentation Conference (IBIC2019), 526 (2019).